Gossamer high-temperature bulk superconductivity in FeSe

A. A. Sinchenko,[1,2] P. D. Grigoriev,[3,4,5,6,*] A. P. Orlov,[1] A. V. Frolov,[1] A. Shakin,[5]
D. A. Chareev,[7,8] O. S. Volkova,[7,9,10] and A. N. Vasiliev[5,9,10]

[1]*Kotel'nikov Institute of Radioengineering and Electronics of RAS, Mokhovaya 11-7, 125009 Moscow, Russia*
[2]*National Research Nuclear University (MEPhI), 115409 Moscow, Russia*
[3]*L.D. Landau Institute for Theoretical Physics, 142432 Chernogolovka, Russia*
[4]*P.N. Lebedev Physical Institute, RAS, 119991, Moscow, Russia*
[5]*National University of Science and Technology "MISiS," 119049 Moscow, Russia*
[6]*Institut Laue-Langevin, 38042, Grenoble, France*
[7]*Ural Federal University, 620002 Ekaterinburg, Russia*
[8]*Institute of Experimental Mineralogy, RAS, 142432 Chernogolovka, Russia*
[9]*M.V. Lomonosov Moscow State University, 119991 Moscow, Russia*
[10]*National Research South Ural State University, 454080 Chelyabinsk, Russia*

(Received 27 October 2016; revised manuscript received 22 March 2017; published 14 April 2017)

Using the anisotropic electron transport and susceptibility measurements we demonstrate the appearance of inhomogeneous gossamer superconductivity in FeSe single crystals at ambient pressure and at temperature five times higher than its zero resistance T_c. We also find and quantitatively describe a general property: If inhomogeneous superconductivity in a anisotropic conductor first appears in the form of isolated superconducting islands, it reduces electric resistivity anisotropically with maximal effect along the least conducting axis. This gives a simple tool to study inhomogeneous superconductivity in various anisotropic compounds, which helps to investigate the onset of high-temperature superconductivity.

DOI: 10.1103/PhysRevB.95.165120

The highest superconducting transition temperature T_c in the most promising copper-oxide and iron-based high-temperature superconductors appears at some nonstoichiometric chemical composition or doping [1,2]. This inevitably leads to a spatial inhomogeneity of these compounds because of local variations of doping level. High-temperature superconductivity in these compounds, possibly, first appears in the form of small isolated superconducting islands, which become connected and coherent with decreasing temperature or with changing another driving parameter, i.e. doping or pressure [3]. Such inhomogeneous superconductivity with disrupted long-range order is often called *gossamer superconductivity*, the term first introduced by Robert Laughlin [4]. Transition to this specific state is supported by the diamagnetic response, observed in various cuprate superconductors far above T_c [5–8]. The numerous direct observation of inhomogeneous electronic structure on a microscopic scale of a few nanometers using STM and other experimental tools was reported in $Bi_2Sr_2CaCu_2O_{8+\delta}$ [9–12], in $HgBa_2CuO_{4+\delta}$ [13], in Fe-based high-Tc superconductor Pr-doped $CaFe_2As_2$ ($T_c \approx 45$ K) [14], etc.

Whether the spatial inhomogeneity is a concomitant or assistant feature of high-temperature superconductivity is still debated, although various theoretical models propose an enhancement of superconducting transition temperature due to such inhomogeneity [3,15]. It is highly desirable to have a general and simple experimental test if superconductivity first appears in the form of isolated islands. The interplay between spin(charge)-density wave and superconductivity may also lead to inhomogeneous superconductivity and even to the anisotropic superconductivity onset, as observed in organic superconductors $(TMTSF)_2PF_6$ and $(TMTSF)_2ClO_4$ [16–18]. This feature looks odd and counterintuitive, however, a similar effect was also reported in the cuprate high-Tc superconductor $YBa_2Cu_4O_8$ [19].

In this paper we formulate, prove, and quantify a general property: If superconductivity in an anisotropic conductor appears in a gossamer form of disconnected superconducting islands, these islands reduce electric resistivity anisotropically, i.e., their influence is first seen in electron transport along the least conducting axis, perpendicular to conducting planes. Using this property we show that superconductivity in bulk FeSe at ambient pressure first appears in the form of isolated islands at temperature $T_c^* \approx 35$–40 K, which is close to superconducting transition temperature at high pressure [20–22] and strongly exceeds the zero-resistance superconducting transition temperature $T_c = 8$ K at ambient pressure [23].

In a layered conductor with the anisotropy parameter $\eta \equiv \sigma_{zz}/\sigma_{xx} \ll 1$ and small superconducting islands of volume ratio $\phi \ll 1$ there are two parallel ways of interlayer current: $j_z \approx j_1 + j_2$ (see Fig. 1), so that the total conductivity $\sigma_{zz}^{tot} \approx \sigma_{zz}^{(1)} + \sigma_{zz}^{(2)}$. The first, standard way is with almost uniform current density and direction $\boldsymbol{j}_1(\boldsymbol{r})$ perpendicular to the conducting layers. The rare superconducting inclusions then only slightly increase corresponding interlayer conductivity $\sigma_{zz}^{(1)}$ proportionally to their volume ratio, and $\sigma_{zz}^{(1)} \sim \eta\sigma_{xx}$. The second way of interlayer current is via superconducting islands. Since these islands are rare, the major part of the current path goes in the normal phase. But instead of flowing along the external field E_z, the current j_2 between the superconducting islands flows along the highly conducting layers until it comes to another island which allows next lift in the interlayer direction. Then there is no local current density along the z axis in the normal phase, and the interlayer conductivity $\sigma_{zz}^{(2)}$ does not acquire the small anisotropy factor

*grigorev@itp.ac.ru

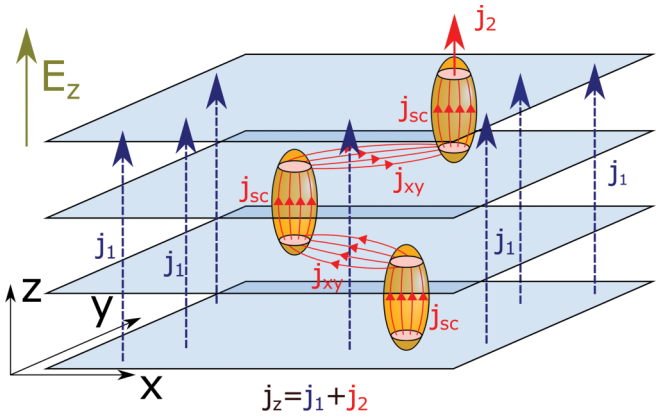

FIG. 1. Illustration of two ways of interlayer current in a heterogeneous media with superconducting inclusions. The first current path j_1, shown by blue dashed arrows, is perpendicular to the conducting layers. The second diffusive path j_2, shown by red solid arrows, goes via superconducting islands and contains long intralayer tracks. The total interlayer current j_z is approximately a sum of these two contributions: $j_z \approx j_1 + j_2$. The yellow ellipsoids illustrate superconducting islands.

η. However, its path along conducting layers between rare superconducting islands is long and inversely proportional to the volume ratio of superconducting phase ϕ, so that $\sigma_{zz}^{(2)} \sim \phi\sigma_{xx}$. Depending on the ratio η/ϕ, the first or the second way makes the main contribution to the interlayer conductivity σ_{zz}^{tot} in such a heterogeneous media.

In the limit of rare superconducting islands, when their volume fraction $\phi \ll 1$, one can apply the Maxwell's approximation (see Sec. 18.1.1 of Ref. [24]), first proposed by Maxwell in 1873 for the isotropic 3D case. Then the isotropic 3D media of conductivity σ_1 with spherical inclusions (granules) of conductivity σ_2 with small volume fraction $\phi \ll 1$ is equivalent to the uniform media with effective conductivity σ_e determined by the linear equation (see Sec. A of Ref. [25] for details)

$$(\sigma_e - \sigma_1)/(\sigma_e + 2\sigma_1) = \phi(\sigma_2 - \sigma_1)/(\sigma_2 + 2\sigma_1), \qquad (1)$$

which gives

$$\frac{\sigma_e}{\sigma_1} = 1 + \frac{3\phi(\sigma_2 - \sigma_1)}{\sigma_2(1-\phi) + \sigma_1(2+\phi)}. \qquad (2)$$

The problem of conductivity in anisotropic media can be mapped to the problem of isotropic media with anisotropic coordinate dilations (see Sec. B of Ref. [25] for details). Thus, the current flow in the media with the easy-plane anisotropy, i.e., where $\sigma_{zz} \ll \sigma_{xx} = \sigma_{yy}$ is similar to the current flow in (mapped) isotropic media with $\sigma_{zz}^* = \sigma_{xx}^* = \sigma_{yy}^* = \sigma_{xx}$ subjected to uniaxial dilation along the z axis: $z_* = z/\sqrt{\eta}$, where $\eta = \sigma_{zz}/\sigma_{xx}$. Then the spherical inclusions inside anisotropic media transform to elongated ellipsoids with axis ratio $a_z/a_x = 1/\sqrt{\eta} \gg 1$ and eccentricity $\chi = \sqrt{1-\eta} \to 1$, which are similar to finite filaments along the c axis. The generalization of Eq. (1) for the mapped media is [24]

$$(1-\phi)(\boldsymbol{\sigma}_e^* - \sigma_1 \boldsymbol{I}) + \frac{\phi(\boldsymbol{\sigma}_e^* - \sigma_2 \boldsymbol{I})}{\boldsymbol{I} + \boldsymbol{A}(\sigma_2 - \sigma_1)/\sigma_1} = 0, \qquad (3)$$

where $\boldsymbol{I}$ is a unitary 3×3 matrix, and the diagonal matrix $\boldsymbol{A}$ for prolate spheroidal ($a_x = a_y$) inclusions is

$$\boldsymbol{A} = \begin{pmatrix} Q & 0 & 0 \\ 0 & Q & 0 \\ 0 & 0 & 1-2Q \end{pmatrix}, \qquad (4)$$

where

$$2Q = 1 + \frac{1}{1/\eta - 1}\left[1 - \frac{1}{2\chi}\ln\left(\frac{1+\chi}{1-\chi}\right)\right]. \qquad (5)$$

For isotropic case $Q = 1/3$, the matrix $\boldsymbol{A} = \boldsymbol{I}/3$, and Eq. (3) simplifies to Eq. (1). For strong anisotropy $\eta = \sigma_{zz}/\sigma_{xx} \ll 1$, the eccentricity $\chi \approx 1 - \eta/2$ is close to unity, and

$$Q \approx 1/2 + \eta[1 + \ln(\eta/4)/2]/2. \qquad (6)$$

Substituting Eq. (4) to Eq. (3) gives the linear matrix equation on $\boldsymbol{\sigma}_e^*$:

$$(1-\phi)(\boldsymbol{\sigma}_e^* - \sigma_1 \boldsymbol{I})[(\boldsymbol{I} - \boldsymbol{A})\sigma_1 + \boldsymbol{A}\sigma_2] + \phi(\boldsymbol{\sigma}_e^* - \sigma_2 \boldsymbol{I})\sigma_1 = 0. \qquad (7)$$

The solution of this equation is the diagonal matrix $\boldsymbol{\sigma}_e^*$. Its three diagonal elements at $\sigma_2/\sigma_1 \to \infty$ simplify to

$$\frac{\sigma_{xx}^*}{\sigma_1} \to \frac{Q(1-\phi)+\phi}{Q(1-\phi)} = 1 + \frac{\phi}{Q(1-\phi)}, \qquad (8)$$

$\sigma_{yy}^* = \sigma_{xx}^*$, and

$$\frac{\sigma_{zz}^*}{\sigma_1} \to \frac{2Q(1-\phi)-1}{(2Q-1)(1-\phi)} = \frac{1}{1-\phi} + \frac{2Q\phi}{(1-2Q)(1-\phi)}. \qquad (9)$$

For strongly anisotropic compounds with $\eta \ll 1$, substituting Eq. (6) and making reverse mapping $z = \sqrt{\eta} z_*$ and $\sigma_{zz} = \eta\sigma_{zz}^*$ to initial problem, from Eqs. (8) and (9) we finally obtain

$$\sigma_{xx} \approx \sigma_1(1 + 2\phi), \qquad (10)$$

and

$$\sigma_{zz} \approx \sigma_1\left(\frac{\eta}{1-\phi} + \frac{\phi}{\ln(2/\sqrt{\eta}) - 1}\right). \qquad (11)$$

The expression (11) for interlayer conductivity σ_{zz} consists of two parts. The first (regular) part at $\phi \ll 1$ only slightly increases, similarly to σ_{xx}. This part corresponds to the usual interlayer transport with local current density j_1 almost perpendicular to conducting layers, so that it contains the small anisotropy factor $\sigma_{zz}/\sigma_{xx} \approx \eta$. The second (irregular) part of σ_{zz} in Eq. (11) corresponds to the strongly nonuniform current density j_2: The current flows via superconducting islands along the z axis and between these superconducting islands along the conducting (x, y) planes (see Fig. 1). This term does not have small anisotropy factor η, but contains another small factor ϕ, the volume fraction of superconducting islands. Hence, at $\phi > \eta$ the resulting conductivity anisotropy due to spherical superconducting islands reduces from $\sigma_{xx}/\sigma_{zz} = 1/\eta \gg 1$ to $\sigma_{xx}/\sigma_{zz} \approx 1/\phi$.

For present experiments we have chosen good quality plate-like single crystals (flakes) of $FeSe_{1-\delta}$ superconductor, grown in evacuated quartz ampoules using AlCl3/KCl flux technique in permanent temperature gradient, as described in Ref. [26].

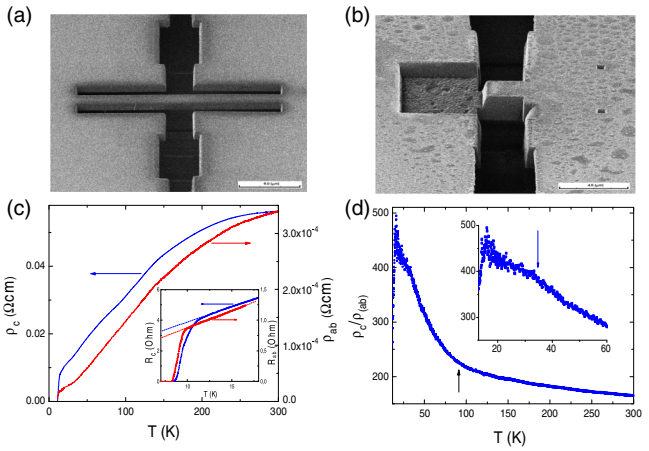

FIG. 2. (a) The SIM image of FeSe in-plane microbridge; (b) The SIM image of FeSe microbridge (overlap structure) oriented along the c axis; (c) temperature dependencies of resistivity: red curve—structure A and blue curve—structure B. Inset shows superconducting transition for both types of structures; (d) Anisotropy of conductivity, ρ_c/ρ_{ab} as a function of temperature.

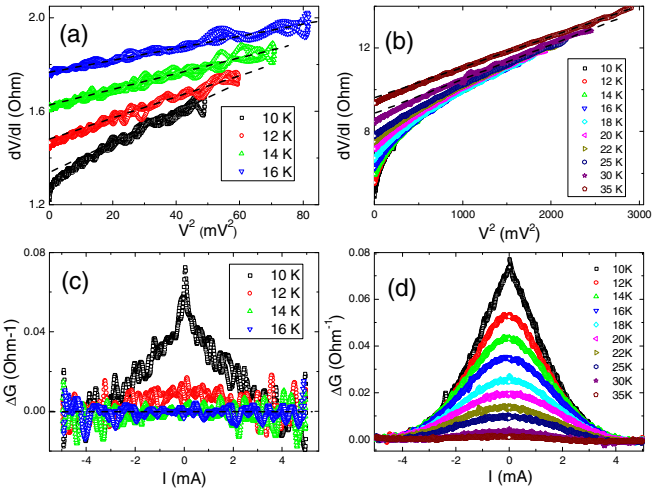

FIG. 3. (a) Differential resistance dV/dI as a function of the square of voltage, V^2, at different temperatures above T_c for A-type structure, i.e., for intralayer transport. (b) The same as (a) but for B-type structure, i.e., for interlayer transport. (c) Excess differential conductivity as a function of current for A-type structure measured at different temperatures above T_c. (d) The same as in (c) but for B-type structure.

The structures of two types have been fabricated by the focused ion beam (FIB) technique described in Ref. [27] from selected thin single-crystal samples with a thickness typically 2–4 μm [see Figs. 2(a) and 2(b)]. Structure of the first type, called below as A type and shown in Fig. 2(a), is an in-plane bridge of length 20 μm, width 2 μm, and thickness equal to single crystal thickness. This bridge is used to measure the intralayer resistance ρ_{ab}. Structure of the second type, shown in Fig. 2(b) and called below as B type, is a bridge oriented transverse to the layers, along the c axis, with typical sizes $L_a \times L_b \times L_c = 2\ \mu\text{m} \times 2\ \mu\text{m} \times 0.2\,\mu\text{m}$. This bridge is used to measure the interlayer resistance ρ_c. All together, the five pairs of both types of structures prepared from the same single crystals have been studied. The electrical contacts to the crystal have been prepared by the laser evaporation of gold films before the processing by FIB. The measurements of electrical resistance and of current-voltage (IV) characteristics have been done in the conventional four-probe configuration. To improve thermal exchange all structures were covered by collodium. The temperature dependence of magnetic susceptibility of FeSe single crystal was obtained by the AC measurement option of the physical property measurement system—9T Quantum Design. The plate was oriented perpendicular to external magnetic field $H = 10$ Oe applied at frequency 10 kHz. The demagnetizing factor $N \sim 0.5$ was supposed to obtain the full Meissner effect $4\pi\chi = -1$ for a finite size plate in accordance with classical formula [28].

Figure 2(c) shows the temperature dependence of resistivity in the structures of both types. The well-defined geometry of these structures allowed us to determine the conductivity anisotropy ratio ρ_c/ρ_{ab} and its temperature evolution, shown in Fig. 2(d). At room temperature $\rho_c/\rho_{ab} \approx 160$–$180$ and increases monotonically with temperature, reaching $\approx$500 at $T = 12$ K. This increase of anisotropy goes in two stages. First, in the temperature range 300–90 K, the rate of this increase is about 0.25–0.30 K^{-1}. Then, below 90 K, this rate increases by one order of magnitude, achieving 2.5–3.0 K^{-1}. This behavior reflects the strong decreasing of interlayer conductivity at temperature below the structural transition [29,30]. Additionally, in Fig. 2(d) one may see a small kink at $T \approx 35$ K. This feature is discussed below in detail.

Taking into account the layered crystal structure of FeSe, in B-type structures one may expect to observe some effects of weak superconductivity, namely, intrinsic Josephson effect, similar to that in layered cuprate high-T_c superconductors [31]. Surprisingly, in our structures we have observed just the opposite picture: Superconductivity is stronger in the direction perpendicular to conducting layers as compared to intralayer superconductivity. Inset in Fig. 2(c) demonstrates superconducting transition for both types of structures. As can be seen, superconducting temperature in B-type structure is higher than in A-type structure. Such a behavior was observed for all studied samples.

The most interesting result was obtained during the study of the IV characteristics of the bridge structures at temperature above T_c. Usually, linear $R(T)$ behavior in a normal metallic state corresponds to the quadratic dependence of differential resistance on voltage at the condition of little change of specific heat in the case of small Joule heating. For superconducting materials one expects small deviations from this square dependence caused by superconducting fluctuations which appear in IV curves as excess conductivity at temperature close to T_c. Let us consider first IV curves for intralayer transport. Figure 3(a) illustrates dV/dI as a function of V^2 at different temperatures above T_c for the A-type structure. One sees that the intralayer electronic transport in A-type structure demonstrates conventional behavior: At high current the differential resistance is a square function of voltage at all measured temperatures, but close to T_c we observed excess conductivity (deviation from square law) at low current corresponding to the superconducting fluctuations which disappear rapidly and are completely absent above $T = 13$ K.

It is important to note that the observation of quadratic dependence of differential resistance on voltage indicates a negligible influence of temperature variation of specific heat during measurements. Figure 3(c) shows corresponding excess conductivity as a function of current, which was obtained by the extracting of normal state quadratic background from the experimental IV curves. This behavior correlates well with $R(T)$ behavior for this type of structures [inset in Fig. 2(c)].

Quite different behavior is observed in the interlayer electronic transport, i.e., in the B-type structure. As can be seen from Figs. 3(b) and 3(d), at high current, as in the case of A-type structures, IV curves follow square dependence but the excess conductivity observed at low current is much more pronounced and, more importantly, observed up to $T \approx 35$ K. Note, that $R(T)$ for this type of junction is also strongly linear at least in the temperature range 14–25 K [see inset in Fig. 2(c)]. In all cases both types of structures (A and B) were prepared on the same single crystal and measured simultaneously at the same thermal conditions, demonstrating nearly the same overheating about 2–3 K for maximal current in different samples. So, the qualitatively different behavior of A and B type structures observed below 35 K cannot be explained by different thermal conditions or by the influence of temperature variation of the specific heat. The difference between intralayer and interlayer conductivity is clearly seen in Fig. 4(a), where we plot the temperature dependence of excess conductivity for both types of structures.

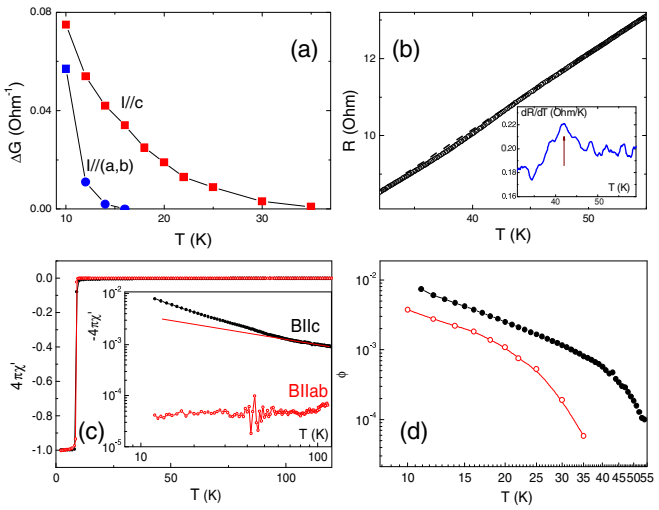

FIG. 4. (a) Temperature dependencies of excess conductivity: red curve with square symbols for the B-type structure, and blue curve with circle symbols for the A-type structure. (b) Temperature dependence of interlayer resistance in the temperature range 30–60 K demonstrating small decrease of resistance at $T \approx 45$ K. Inset shows derivative of this curve. (c) The temperature dependence of the real part of magnetic susceptibility of FeSe single crystal obtained for magnetic field B applied parallel to the ab plane (open circles) and perpendicular to the plane (closed circles). Main panel contains initial $4\pi\chi$ curve obtained for demagnetizing factor $N \sim 0.5$ for $B \parallel c$ and $N = 0$ for $B \parallel ab$, and the inset represents the same curve in double logarithmic scale to highlight the negative deviation at high temperatures. The line is a guide for the eye. (d) The temperature dependencies of superconducting phase percentage obtained from $B \parallel c$ magnetic (closed circles) and from transport (open circles) measurements using Eq. (11).

The explanation for the observed excess conductivity in interlayer transport by simple fluctuation effects seems unrealistic. We see now only one explanation of the observed effect: the formation of small superconducting islands with $T_c^* \approx 35$–40 K. Then at $T = T_c^*$ the corresponding decrease of resistance $R(T)$ should be anisotropic according to the above theoretical model. The experimental fact that the superconducting fluctuations in FeSe are much stronger and distinctly different from those in conventional superconductors has already been reported [32] and interpreted in terms of preformed Cooper pairs without long-range coherence, which is close to our interpretation of spatially separated superconducting islands.

Our results are in agreement with the recent work [33] where a rise in T_c more than twice was observed in point contacts between FeSe single crystal and Cu. The point contact was formed between cooper wire and the plane of FeSe crystal. It is well known that the point contact itself is directional with respect to the electric-field configuration [34], and one may expect that the main contribution to the point-contact resistance comes from injection along the point-contact orientation, making point contact configuration close to our experimental geometry. Then the authors of Ref. [33] probed the electronic transport mainly along the c axis and, therefore, observed a similar effect from the filamentary gossamer superconductivity.

We observe small peculiarities already in the $R(T)$ dependencies which may indicate the appearance of superconducting islands. A very small but visible decrease of interlayer resistance can be noticed at $T \approx 42$–45 K as shown in Fig. 4(b). This effect is more pronounced in the derivative curve, $dR/dT(T)$, shown in the inset to Fig. 4(b). Note that this feature is completely absent in the intralayer resistance. As one can see in the inset in Fig. 2(d), at nearly the same temperature some decrease of anisotropy is also observed.

In the present work we also measured the magnetic properties of studied crystals. The temperature dependence of the real part of magnetic susceptibility $4\pi\chi$ shown in Fig. 4(c) demonstrates a negative deviation in the whole temperature range for $B \parallel c$. At high temperatures it decreases almost linearly then bends down at approximately 50 K which can be seen more clearly in double logarithmic scale shown in the inset to Fig. 4(c), and finally drops to absolute diamagnetic value $4\pi\chi = -1$ below superconducting phase transition $T_C = 9$ K. The rough estimation of superconducting phase portion ϕ can be done by subtraction of linear function from $4\pi\chi(T)$ dependence assuming 100% of superconducting phase at low temperatures $T \ll T_C$. The temperature dependencies of superconducting phase percentage obtained from magnetic (closed circles) and transport (open circles) measurements are shown in Fig. 4(d). In the latter case, the volume fraction ϕ of superconducting phase was calculated from Eq. (11) using the experimental data on conductivity anisotropy, shown in Fig. 2(d). Figure 4(d) shows that ϕ is very small and decreases monotonically with increasing temperature. It is distinguishable below 50 K and amounts to 10^{-4} at this temperature. At lower temperatures it is somewhat higher and comprises 10^{-2} above T_c . The shape of $\phi(T)$ dependence

obtained from magnetic measurements is similar to that from transport measurements [see Fig. 4(d)]. Measurements of transport and magnetic properties for $I \parallel ab$ or $B \parallel ab$ contain practically no indications of excess conductivity [Fig. 4(a)] or negative deviation in magnetic susceptibility [Fig. 4(c)], because for this direction the current flows only along the highly conductive ab layers and does not contain the transport along the c axis.

In conclusion, we report the discovery of inhomogeneous superconductivity in bulk $FeSe_{1-\delta}$ at ambient pressure and at temperature $T_c^* \sim 35$ K, which is five times higher than its zero-resistance superconducting transition temperature $T_c \approx 8$ K known before Ref. [23]. This superconductivity appears in the form of microscopic isolated superconducting islands and does not lead to zero electric resistance but reveals itself in anisotropic resistivity drop and in magnetic susceptibility. Complementary, we proposed and described a general property: If inhomogeneous superconductivity in an anisotropic conductor first appears in the form of isolated superconducting islands, it reduces electric resistivity anisotropically with maximal effect along the least conducting axis. This property provides a simple and very general tool to detect inhomogeneous superconductivity in various anisotropic compounds, and this method may be applicable to almost all high-temperature superconductors which have layered anisotropic crystal structure.

P.G. thanks Dmitrii Lyubshin for useful discussion. This work was supported in part by the Ministry of Education and Science of the Russian Federation in the framework of Increase Competitiveness Program of NUST MISiS #K2-2016-066, by RFBR #16-02-00522, and by Act 211 of Government of the Russian Federation, contracts 02.A03.21.0006 and 02.A03.21.0011. The theoretical part was supported by Russian Science Foundation # 16-42-01100.

[1] B. Keimer, S. A. Kivelson, M. R. Norman, S. Uchida, and J. Zaanen, Nature (London) **518**, 179 (2015).
[2] Qimiao Si, Rong Yu, and Elihu Abrahams, Nat. Rev. Mater. **1**, 16017 (2016).
[3] V. Z. Kresin, Yu. N. Ovchinnikov, and S. A. Wolf, Phys. Rep. **431**, 231 (2006).
[4] R. B. Laughlin, Philos. Mag. **86**, 1165 (2006).
[5] I. Iguchi, T. Yamaguchi, and A. Sugimoto, Nature (London) **412**, 420 (2001).
[6] C. Bergemann, A. W. Tyler, A. P. Mackenzie, J. R. Cooper, S. R. Julian, and D. E. Farrell, Phys. Rev. B **57**, 14387 (1998).
[7] P. Carretta, A. Lascialfari, A. Rigamonti, A. Rosso, and A. Varlamov, Phys. Rev. B **61**, 12420 (2000).
[8] A. Lascialfari, A. Rigamonti, L. Romano, P. Tedesco, A. Varlamov, and D. Embriaco, Phys. Rev. B **65**, 144523 (2002).
[9] S. H. Pan, J. P. O'Neal, R. L. Badzey, C. Chamon, H. Ding, J. R. Engelbrecht, Z. Wang, H. Eisaki, S. Uchida, A. K. Gupta, K.-W. Ng, E. W. Hudson, K. M. Lang, and J. C. Davis, Nature (London) **413**, 282 (2001).
[10] K. M. Lang, V. Madhavan, J. E. Hoffman, E. W. Hudson, H. Eisaki, S. Uchida, and J. C. Davis, Nature (London) **415**, 412 (2002).
[11] K. K. Gomes, A. N. Pasupathy, A. Pushp, S. Ono, Y. Ando, and A. Yazdani, Nature (London) **447**, 569 (2007).
[12] W. D. Wise, Kamalesh Chatterjee, M. C. Boyer, Takeshi Kondo, T. Takeuchi, H. Ikuta, Zhijun Xu, Jinsheng Wen, G. D. Gu, Yayu Wang, and E. W. Hudson, Nat. Phys. **5**, 213 (2009).
[13] G. Campi, A. Bianconi, N. Poccia, G. Bianconi, L. Barba, G. Arrighetti, D. Innocenti, J. Karpinski, N. D. Zhigadlo, S. M. Kazakov, M. Burghammer, M. v. Zimmermann, M. Sprung, and A. Ricci, Nature (London) **525**, 359 (2015).
[14] Krzysztof Gofryk, Minghu Pan, Claudia Cantoni, Bayrammurad Saparov, Jonathan E. Mitchell, and Athena S. Sefat, Phys. Rev. Lett. **112**, 047005 (2014).
[15] I. Martin, D. Podolsky, and S. A. Kivelson, Phys. Rev. B **72**, 060502(R) (2005).
[16] N. Kang, B. Salameh, P. Auban-Senzier, D. Jerome, C. R. Pasquier, and S. Brazovskii, Phys. Rev. B **81**, 100509(R) (2010).
[17] Arjun Narayanan, Andhika Kiswandhi, David Graf, James Brooks, and Paul Chaikin, Phys. Rev. Lett. **112**, 146402 (2014).
[18] Ya. A. Gerasimenko, S. V. Sanduleanu, V. A. Prudkoglyad, A. V. Kornilov, J. Yamada, J. S. Qualls, and V. M. Pudalov, Phys. Rev. B **89**, 054518 (2014).
[19] N. E. Hussey, K. Nozawa, H. Takagi, S. Adachi, and K. Tanabe, Phys. Rev. B **56**, R11423 (1997).
[20] Yoshikazu Mizuguchi, Fumiaki Tomioka, Shunsuke Tsuda, Takahide Yamaguchi, and Yoshihiko Takano, Appl. Phys. Lett. **93**, 152505 (2008).
[21] S. Medvedev, T. M. McQueen, I. A. Troyan, T. Palasyuk, M. I. Eremets, R. J. Cava, S. Naghavi, F. Casper, V. Ksenofontov, G. Wortmann, and C. Felser, Nat. Mater. **8**, 630 (2009).
[22] J. P. Sun, K. Matsuura, G. Z. Ye, Y. Mizukami, M. Shimozawa, K. Matsubayashi, M. Yamashita, T. Watashige, S. Kasahara, Y. Matsuda, J.-Q. Yan, B. C. Sales, Y. Uwatoko, J.-G. Cheng, and T. Shibauchi, Nat. Commun. **7**, 12146 (2016).
[23] F.-C. Hsu, Jiu-Yong Luo, K.-W. Yeh, T.-K. Chen, T.-W. Huang, P. M. Wu, Y.-C. Lee, Y.-L. Huang, Y.-Y. Chu, D.-C. Yan, and M.-K. Wu, PNAS **105**, 14262 (2008).
[24] S. Torquato, *Random Heterogeneous Materials* (Springer, New York, 2002).
[25] See Supplemental Material at http://link.aps.org/supplemental/10.1103/PhysRevB.95.165120 for theoretical derivation of the dilatation mapping to isotropic problem and of Eq. (1) in the Maxwell's approximation for spherical inclusions, and for additional experimental data obtained on another sample to show the reproducibility of main results.
[26] D. Chareev, E. Osadchii, T. Kuzmicheva, J. Y. Lin, S. Kuzmichev, O. Volkova, and A. Vasiliev, Cryst. Eng. Comm. **15**, 1989 (2013).
[27] Yu. I. Latyshev, P. Monceau, A. A. Sinchenko, L. N. Bulaevskii, S. A. Brazovskii, T. Kawae, and T. Yamashita, J. Phys. A: Math. Gen. **36**, 9323 (2003).
[28] R. B. Goldfarb, M. Lelental, and C. A. Thompson, in *Magnetic Susceptibility of Superconductors and Other Spin Systems*, edited by R. A. Hein, T. L. Francavilla, and D. H. Liebenberg (Plenum, New York, 1991), pp. 49–80.

[29] T. M. McQueen, A. J. Williams, P. W. Stephens, J. Tao, Y. Zhu, V. Ksenofontov, F. Casper, C. Felser, and R. J. Cava, Phys. Rev. Lett. **103**, 057002 (2009).

[30] T. Terashima, N. Kikugawa, S. Kasahara, T. Watashige, T. Shibauchi, Y. Matsuda, T. Wolf, A. E. Böhmer, F. Hardy, C. Meingast, H. v. Löhneysen, and S. Uji, J. Phys. Soc. Jpn. **84**, 063701 (2015).

[31] R. Kleiner and P. Muller, Phys. Rev. B **49**, 1327 (1994).

[32] S. Kasahara, T. Yamashita, A. Shi, R. Kobayashi, Y. Shimoyama, T. Watashige, K. Ishida, T. Terashima, T. Wolf, F. Hardy, C. Meingast, H. v. Lohneysen, A. Levchenko, T. Shibauchi, and Y. Matsuda, Nat. Commun. **7**, 12843 (2016).

[33] Yu. G. Naidyuk, G. Fuchs, D. A. Chareev, and A. N. Vasiliev, Phys. Rev. B **93**, 144515 (2016).

[34] A. A. Sinchenko and P. Monceau, Phys. Rev. B **67**, 125117 (2003).